CrossMark

RESEARCH PAPER

Fractionating power and outlet stream polydispersity in asymmetrical flow field-flow fractionation. Part II: programmed operation

P. Stephen Williams[1]

Abstract Asymmetrical flow field-flow fractionation (As-FlFFF) is a widely used technique for analyzing polydisperse nanoparticle and macromolecular samples. The programmed decay of cross flow rate is often employed. The interdependence of the cross flow rate through the membrane and the fluid flow along the channel length complicates the prediction of elution time and fractionating power. The theory for their calculation is presented. It is also confirmed for examples of exponential decay of cross flow rate with constant channel outlet flow rate that the residual sample polydispersity at the channel outlet is quite well approximated by the reciprocal of four times the fractionating power. Residual polydispersity is of importance when online MALS or DLS detection are used to extract quantitative information on particle size or molecular weight. The theory presented here provides a firm basis for the optimization of programmed flow conditions in As-FlFFF.

Keywords Asymmetrical flow field-flow fractionation · Programmed operation · Fractionating power · Outlet stream polydispersity

Symbols

b_z	Channel breadth at distance z from channel inlet
d	Particle diameter
d_i	Projected inversion diameter

✉ P. Stephen Williams
p.stephen.williams@gmail.com

[1] Cambrian Technologies Inc., 1772 Saratoga Avenue, Cleveland, OH 44109, USA

$\overline{d}_n$	Number average particle diameter
D	Translational diffusion coefficient
F_d	Particle-diameter-based fractionating power
F_M	Molecular-weight-based fractionating power
F_ϕ	ϕ-based fractionating power
f	Final fraction of time interval required for peak center of mass to reach channel outlet
f	Ratio of d to d_i
$H_{neq}(z, t)$	Non-equilibrium plate height at distance z from channel inlet at time t
L	Length of channel measured from inlet to outlet
M	Molecular weight
N_m	Limiting number of theoretical plates due to the multipath effect in isocratic elution
$R(t)$	Retention ratio at time t
R_c	Core retention ratio
R_s	Resolution
S_d	Diameter-based selectivity
S_M	Molecular-weight-based selectivity
S_ϕ	ϕ-based selectivity
t	Time
t_r	Elution time from focusing point to channel outlet
t_1	Pre-decay time
$\langle v(z, t) \rangle$	Mean channel flow velocity at distance z from inlet and at time t
V	Volume of channel measured from the inlet up to distance z
$\dot{V}(z, t)$	Volumetric flow rate at distance z from channel inlet at time t
$\dot{V}(V, t)$	Volumetric flow rate at fractional channel volume V measured from the inlet at time t
$\dot{V}_B$	Backward flow rate applied to the outlet during sample introduction and focusing
$\dot{V}_c(t)$	Volumetric flow rate through the membrane at time t

$\dot{V}_{c0}$	Initial volumetric flow rate through the membrane
$\dot{V}_F$	Forward flow rate applied to the inlet during sample introduction and focusing
$\dot{V}_L$	Constant outlet flow rate
V^0	Effective void volume measured from focusing point to channel outlet
V_C^0	Channel volume
w	Channel thickness
z	Distance from channel inlet
z'	Distance of sample focusing point from channel inlet
α	Ratio of the exclusion distance from the wall to the channel thickness
ε	Small multiplicative correction to δt yielding $t_r - \sigma_{t,m}$
λ_c	Core retention parameter
$\lambda_0(t)$	Retention parameter at time t
σ_d	Standard deviation in number distribution of particle diameter
$\sigma_{d,app}$	Apparent σ_d calculated using Eq. 47
σ_t	Standard deviation in retention time
$\sigma_{t,m}$	Standard deviation in retention time due to the multipath effect
$\sigma_{t,neq}$	Standard deviation in retention time due to the nonequilibrium effect
σ_z	Standard deviation in distance traveled
τ	Exponential decay time constant for programmed cross flow rate
ϕ	Selective parameter such as d or M
$\chi(t)$	Non equilibrium bandspreading parameter at time t
χ_c	Core nonequilibrium bandspreading parameter

Introduction

Compared to other particle or polymer separation techniques, such as size exclusion or gel permeation chromatography, the field-flow fractionation (FFF) techniques tend to give greater relative differences in elution time for small relative differences in particle size or molecular weight. In the terminology of separation science, they exhibit higher selectivity. While this can be advantageous for the separation of a small number of slightly different species, it can lead to difficulties in the analysis of widely polydisperse samples. Conditions suitable for sufficient retention and resolution of the smaller components can result in excessive retention of the larger components. In the case of sedimentation FFF (SdFFF), the selectivity is so high that there may also be difficulty in detection of the larger components as they are eluted over extended periods of time with consequent dilution in the outlet stream. It is also possible that conditions giving sufficient retention for the smaller components result in the interference of steric inversion in the elution of the larger components. The continuous

programmed reduction of field strength during sample elution takes care of these problems by effectively reducing the selectivity in a controlled manner [1, 2].

The technique of symmetrical flow field-flow fractionation (Sym-FlFFF) was introduced in 1976 [3–5] and the asymmetrical form (As-FlFFF) in 1986 [6, 7]. The selectivity of FlFFF is not as high as that of SdFFF, but it was confirmed using Sym-FlFFF that a programmed decay of cross flow rate is advantageous for the analysis of samples consisting of components having widely differing sizes [8, 9]. The nature of Sym-FlFFF allowed the cross flow rate to be programmed independently of the channel flow rate, which was usually held constant. It also allowed the channel flow rate to be programmed, if desired. Dual programming of cross flow and channel flow was demonstrated to be advantageous for sample analysis in the hyperlayer mode of operation [10], for example. Hyperlayer and steric modes of operation are not of concern here. In this publication, attention is confined to the normal or Brownian mode, applicable to submicron particles and macromolecules. The independence of the cross flow rate and the channel flow rate in Sym-FlFFF allows not only freedom in the selection of flow rate conditions but also the relatively simple prediction of elution time and fractionating power as a function of particle size or molecular weight for various programmed cross flow decay functions of time [11–14]. This is not the case for As-FlFFF.

In As-FlFFF, only the accumulation wall is permeable and the fluid flowing through the membrane-covered accumulation wall and channel outlet originates at the channel inlet. It follows that, when some of the fluid exits through the membrane, and it is assumed to exit with uniform membrane flux, the volumetric flow rate must decrease along the length of the channel. This form of FlFFF was named asymmetrical FlFFF because of its characteristic flow configuration—the flow-through the membrane is not matched by an equal flow through an opposite permeable wall, and the inlet and outlet flow rates are not equal. The interdependence of the channel inlet and outlet flow rates and the cross flow rate make the selection of suitable experimental conditions more complicated than for Sym-FlFFF. This is particularly true for programmed conditions where even the prediction of elution times becomes non-trivial. In spite of these difficulties, it has become the dominant form of FlFFF because it eliminates problems associated with the permeable frit that serves as the depletion wall in Sym-FlFFF. The flow through the frit may be non-uniform due to variations in its porosity and due to the pressure drop along the length of the channel under elution conditions. The ultrafiltration membrane, offering a much higher hydraulic resistance than the frit, requires a greater pressure drop across its thickness to maintain the cross flow. The much lower pressure drop along the channel length therefore has relatively little effect on the uniformity of membrane flux. However, the variation in frit flow due to the decreasing

pressure along the channel can result in reduced channel flow rate and higher retention times than expected. The effect is related to that described by Martin and Hoyos for the "no-field method" for void time determination in FlFFF [15].

For an As-FlFFF channel of constant breadth, the flow velocity along the channel length necessarily decreases from the inlet to the outlet as fluid is lost through the accumulation wall. This can lead to problems in particle elution due to non-idealities such as particle interactions with the membrane surface. These interactions may increase as channel flow velocity decreases, and some of the more retained particles may not elute. The loss of volumetric flow rate along the channel length may be partially compensated by gradually reducing the channel breadth along its length. In 1991, Wahlund and Litzén introduced the trapezoidal channel in which the channel breadth decreases linearly [16], and in 1997 an exponentially decreasing channel breadth was proposed for use in As-FlFFF [17]. The variation in mean channel flow velocity along the length of these channels can be greatly reduced compared to a rectangular channel. Under conditions of programmed cross flow rate, the ratio of inlet to outlet flow rate is continuously changing. The ratio, initially high, approaches unity as cross flow rate approaches zero. A decreasing channel breadth remains advantageous for programmed operation as the ratio of inlet to outlet flow rate is likely to be considerably greater than unity for much of the time.

It was mentioned above that in Sym-FlFFF, the cross flow rate may be programmed independently of the channel flow rate which may be held constant or programmed as desired. This is not the case for As-FlFFF. The sum of the volumetric flow rates through the membrane and the channel outlet at any instant must equal the volumetric flow rate at the inlet. The programmed reduction of flow rate through the membrane may be carried out while maintaining a constant channel outlet flow rate, in which case the flow rate at the channel inlet must decrease at the same quantitative rate as the cross flow. This approach has the advantage of not requiring detector signal baseline adjustment, compensation for flow rate change through concentration-sensitive detectors, or compensation for change in delay times between multiple detectors. The programmed decay of cross flow rate may alternatively be carried out while maintaining constant channel inlet flow rate, which would result in an increasing channel outlet flow rate. It is also possible to program either the inlet or outlet flow rate along with the cross flow rate, the non-programmed flow being consistent with the difference or sum of the other two, respectively.

The programming of flow rates in rectangular-channel As-FlFFF was first carried out by Litzén and Wahlund in 1989 for the separation of human serum albumin from its dimer and trimer [18]. They used a multistep program where the ratio of cross flow rate to outlet flow rate was reduced in six abrupt steps while the channel inlet flow rate was held constant. The outlet flow rate therefore increased in stepwise fashion during programming. The first peak, corresponding to the monomer, did not elute until the cross flow program was completed and baseline correction was not therefore required. They also used a simple single-step program to separate two plasmid fragments of 700 and 4600 bp. In this case, the cross flow rate was reduced to zero following elution of the first peak.

In 1992, Kirkland et al. [19] used an exponential decay of cross flow rate in rectangular-channel As-FlFFF to separate a mixture of proteins and nucleic acids, a bacteria sample, and a mixture of submicron silica particles. They elected to hold the channel outlet flow rate constant to avoid baseline drift and to maintain constant detector response for quantification purposes. They were able to derive an analytical expression for elution time as a function of diffusion coefficient based on a simple high retention approximation for retention ratio (this is discussed later in this manuscript).

In 2001, Moon and Hwang [20] gave an example of a separation of four proteins obtained under linearly programmed decay of cross flow rate with the outlet flow rate held constant. Also in 2001, Moon [21] showed two more examples of separations obtained under linear decay of cross flow. In 2002, Moon et al. [22] applied a variety of flow programs to As-FlFFF using a trapezoidal channel. They were able to show how approximate analytical solutions were derivable for retention times with exponentially programmed cross flow rate and constant or exponentially programmed outlet flow rate, and that the solutions were independent of the channel breadth profile. A mixture of polystyrene sulfonate standards was separated under a variety of conditions, including isocratic, linear decay of cross flow rate with constant outlet flow rate, linear decay of cross flow rate with linearly increasing outlet flow rate (and linearly decreasing inlet flow rate), and power programmed decay of cross flow rate with constant, linearly increasing, and linearly decreasing outlet flow rate. In cases where outlet flow rate varied, a baseline correction was applied. The programming of outlet flow rate was seen to influence sample elution to a much smaller extent than the decay of cross flow rate.

In 2004, Andersson et al. [23] used successive intervals of decreasing gradients of linear decay of cross flow rate to fractionate ethyl hydroxyethyl cellulose samples. In 2006, Leeman et al. [24] published a comparison of various linear and exponential cross flow decay functions for the separation of mixtures of pullulan standards, paying particular attention to the effect of the rate of decay on the observed selectivity.

Since these early studies, the implementation of programmed decay of cross flow rate in As-FlFFF has become very common. The conditions are generally selected by trial

and error or by reference to previous analyses, and the characterization of the fractionated samples commonly relies on a secondary technique, such as flow-through multi-angle light scattering (MALS) or dynamic light scattering (DLS) applied to the eluent, rather than on fundamental FFF theory. While the use of these secondary techniques for characterizing the fractionated samples compensates for uncertainties in effective channel void volume as well as various non-idealities, such as those due to sample–membrane interactions, the quality of the separation depends on the selected flow conditions. The capacity of a separation system to resolve the components of a polydisperse sample can be quantified in terms of the fractionating power. It provides a measure of the relative resolution that can be obtained across the breadth of the sample [11]. A modeling of elution time and fractionating power in As-FlFFF is therefore necessary for a logical and systematic optimization of separation conditions. This objective was accomplished for constant flow conditions in part I [25] and is accomplished for programmed cross flow rate conditions in the work presented here.

It was shown in part I [25] that, in the case of isocratic analysis of a polydisperse sample by As-FlFFF, the residual channel outlet polydispersity is inversely related to the predicted fractionating power. This relationship supports the use of predicted fractionating power as a criterion for the selection of optimum flow rate conditions because the return of reliable particle size or molecular weight by light scattering detection software depends upon low outlet polydispersity across the full range of the sample. It will be shown in this manuscript that the relationship between outlet polydispersity and fractionating power is also valid for conditions of programmed cross flow rate. The predicted fractionating power is therefore key to the optimization of programmed conditions in As-FlFFF. The consideration of fractionating power is particularly important for programmed decay of cross flow rate as the cross flow may be programmed in any number of ways, as may be seen from the earlier discussion. The selection of the optimum type of cross flow decay program (mathematical function of time) as well as the rate of decay and the magnitude of the channel flow rate may be made based upon the predicted relationship between fractionating power and particle size or molecular weight. It will be shown in this manuscript how fractionating power may be calculated for any programmed decay of cross flow or, in fact, for any arbitrary decrease of cross flow rate with time during sample elution.

Fractionating power

As mentioned above, the fractionating power is used to quantify the relative resolving power of the FFF system for polydisperse samples. If ϕ represents a selective sample property,

such as particle diameter d or molecular weight M, then the ϕ-based fractionating power is defined by [11]

$$F_\phi = \frac{R_s}{\delta\phi/\phi} = \frac{\phi}{4\sigma_t}\frac{\delta t_r}{\delta\phi} \tag{1}$$

where R_s is the resolution, $\delta t_r/4\sigma_t$, between sample components having ϕ that differ by the small relative amount $\delta\phi/\phi$, whose retention times consequently differ by δt_r, and have a mean standard deviation in retention time of σ_t. In the limit of $\delta\phi/\phi \to 0$, Eq. 1 reduces to

$$F_\phi = \frac{\phi}{4\sigma_t}\frac{dt_r}{d\phi} = \frac{t_r}{4\sigma_t}S_\phi \tag{2}$$

where S_ϕ is the ϕ-based selectivity given by

$$S_\phi = \frac{\phi}{t_r}\frac{dt_r}{d\phi} = \frac{d\ln t_r}{d\ln\phi} \tag{3}$$

For isocratic operation, Eq. 2 may also be written in the form $F_\phi = \sqrt{N}S_\phi/4$, where N is the number of theoretical plates ($= t_r^2/\sigma_t^2$); this is not the case for programmed operation. The fractionating power F_ϕ is therefore a continuous function of ϕ. In order to predict fractionating power, it is necessary to predict both t_r and σ_t as functions of ϕ. When particles or molecules are negligibly small, and when particle–particle and particle–membrane interactions are also negligible, the fundamental theory of FFF allows accurate prediction of the retention ratio R, the ratio of mean particle migration velocity to mean fluid velocity at any point in the channel [7]. Finite particle or molecular size can also be approximately accounted for using a first-order steric exclusion correction [26, 27]. For isocratic conditions, a knowledge of the void time then allows prediction of t_r. The method for predicting t_r under programmed conditions is described below.

There are two dominant contributions to bandspreading in As-FlFFF: the nonequilibrium and the multipath contributions. The nonequilibrium contribution is predictable using fundamental FFF theory [27–29], which may also include a steric exclusion correction for finite particle or molecular size [26, 27, 30]. The multipath contribution is the result of small variations in membrane permeability and channel thickness [25] and must be experimentally determined for each assembled channel. It is described below how the contributions to variance in retention time due to these effects may be predicted for programmed conditions.

Volumetric flow rates and mean channel flow velocities along channel length

The same assumptions and approximations regarding the uniformity of fluid flow in the channel are made here as were

made in part I [25]. Particle–particle and particle–membrane interactions are also assumed to be negligible. In addition, the secondary relaxation effect due to the changing cross flow rate during sample elution [31–34] is not considered in this manuscript.

In programmed operation, the flow rate through the accumulation wall $\dot{V}_c$ is a function of time. It may be held constant for a certain initial period, after which it is generally reduced according to some continuous function of time. It may alternatively be reduced in stepwise fashion or in a series of function segments. When the cross flow rate is being reduced, either the channel inlet or outlet flow rate, or possibly both, may vary. Conservation of mass will always demand that

$$\dot{V}_c(t) = \dot{V}(0,t) - \dot{V}(L,t) \tag{4}$$

where $\dot{V}_c(t)$ is the cross flow rate at time t and $\dot{V}(0,t)$ and $\dot{V}(L,t)$ are the flow rates at the channel inlet (at $z = 0$, where z is the distance measured from the channel inlet) and outlet (at $z = L$) at time t, respectively. The local volumetric channel flow rate $\dot{V}$ will be a function of both the distance z from the channel inlet and time t and is given by

$$\dot{V}(z,t) = \dot{V}(0,t) - \frac{\dot{V}_c(t)\,w}{V_C^0} \int_0^z b_z \, dz \tag{5}$$
$$= \dot{V}(L,t) + \dot{V}_c(t) \left(1 - \frac{w}{V_C^0} \int_0^z b_z \, dz \right)$$

in which w is the channel thickness, V_C^0 is the channel volume, and b_z is the channel breadth at distance z from the inlet. Note that Eq. 5 assumes that the membrane flux is uniform throughout the channel. The local mean channel flow velocity $\langle v \rangle$ is then given by

$$\langle v(z,t) \rangle = \frac{\dot{V}(z,t)}{wb_z} \tag{6}$$

Local volumetric channel flow rate can also be given as a function of channel volume V measured from the inlet to distance z from the inlet, such that $V = w \int_0^z b_z \, dz$, and expressed in the form

$$\dot{V}(V,t) = \dot{V}(0,t) - \dot{V}_c(t) \frac{V}{V_C^0} = \dot{V}(L,t) + \dot{V}_c(t) \left(1 - \frac{V}{V_C^0} \right) \tag{7}$$

It will be shown below how the use of Eq. 7 holds certain advantages over that of Eq. 5.

Approximate analytical solutions for retention time

It was shown by Kirkland et al. [19] that an approximate analytical solution for retention time is obtainable in the case of As-FlFFF using constant breadth channels with constant channel outlet flow rate and exponential decay of cross flow rate. They considered only the time-delayed exponential (TDE) program, where the initial constant cross flow period t_1 is equal to the exponential decay constant τ, and the simple exponential decay program with $t_1 = 0$. It was later shown by Moon et al. [22] that an approximate analytical solution could be obtained for As-FlFFF with channels of arbitrary breadth profile, exponential decay of cross flow rate with arbitrary t_1, and outlet volumetric flow rate held constant or exponentially programmed. This was shown to be the case by considering the progress of a zone in terms of the fraction of the channel volume that has been passed through rather than the distance covered, as considered by Kirkland et al. [19]. The local rate at which channel volume is passed through by the center of mass of a monodisperse zone is given by

$$\frac{dV}{dt} = R(t)\,\dot{V}(V,t) = R(t) \left(\dot{V}(L,t) + \dot{V}_c(t) \left(1 - \frac{V}{V_C^0} \right) \right) \tag{8}$$

where $R(t)$ is the time-dependent retention ratio. The strong retention approximation for retention ratio is given by

$$R(t) = 6\lambda_0(t) + 6\alpha = \frac{6DV_C^0}{w^2 \dot{V}_c(t)} + 6\alpha \tag{9}$$

in which $\lambda_0(t)$ is the $\dot{V}_c(t)$-dependent and therefore time-dependent retention parameter (equal to $DV_C^0/w^2\dot{V}_c(t)$), D is the particle or molecule diffusion coefficient, and α is the ratio of the exclusion distance for the particle or molecule center from the wall to the channel thickness. Substituting Eq. 9 into Eq. 8, and rearranging, results in the ordinary differential equation

$$\frac{dV}{dt} + \left(\frac{6D}{w^2} + \frac{6\alpha \dot{V}_c(t)}{V_C^0} \right) V = \left(\frac{6DV_C^0}{w^2} + 6\alpha \dot{V}_c(t) \right) \left(\frac{\dot{V}(L,t)}{\dot{V}_c(t)} + 1 \right) \tag{10}$$

and the solution of this equation is given by

$$V = \exp\left(-\int_0^t \left(\frac{6D}{w^2} + \frac{6\alpha \dot{V}_c(t)}{V_C^0} \right) dt \right)$$
$$\times \left\{ V_C^0 - V^0 + \int_0^t \exp\left(\int_0^t \left(\frac{6D}{w^2} + \frac{6\alpha \dot{V}_c(t)}{V_C^0} \right) dt \right) \left(\frac{6DV_C^0}{w^2} + 6\alpha \dot{V}_c(t) \right) \left(\frac{\dot{V}(L,t)}{\dot{V}_c(t)} + 1 \right) dt \right\} \tag{11}$$

In this equation, V^0 is the effective void volume for particle elution measured from the initial sample focusing point to the

channel outlet. The initial V corresponding to $t = 0$ is therefore equal to $V_C^0 - V^0$. It has been shown [25] that V^0 is given by

$$V^0 = \frac{\dot{V}_B}{\dot{V}_F + \dot{V}_B} V_C^0 \qquad (12)$$

where $\dot{V}_F$ and $\dot{V}_B$ are the forward and backward flow rates during sample introduction and focusing, respectively. Equation 11 does not yield an analytical solution for any simple cross flow decay functions. The result is considerably simplified, however, if α is negligibly small:

$$V = \exp\left(-\frac{6Dt}{w^2}\right)\left\{V_C^0 - V^0 + \frac{6DV_C^0}{w^2}\int_0^t \exp\left(\frac{6Dt}{w^2}\right)\left(\frac{\dot{V}(L,t)}{\dot{V}_c(t)} + 1\right)dt\right\} \qquad (13)$$

Equation 13 may be solved for elution time t_r corresponding to the time at which $V = V_C^0$ for certain programmed flow conditions. For example, it may be solved for the case of constant channel outlet flow rate $\dot{V}_L$ and exponential decay of channel cross flow rate described by

$$\dot{V}_c(t) = \dot{V}_{c0}\exp\left(-\frac{(t-t_1)}{\tau}\right) \qquad (14)$$

in which t_1 is a pre-decay time period during which the cross flow rate is held constant at the initial rate of $\dot{V}_{c0}$ and τ is the exponential decay constant. When $t_r \leq t_1$, elution takes place under constant cross flow conditions, and the solution for t_r is given by

$$t_r = \frac{w^2}{6D}\ln\left(1 + \frac{V^0\dot{V}_{c0}}{V_C^0\dot{V}_L}\right) \qquad (15)$$

When $t_r > t_1$, the solution is given by

$$t_r = t_1 + \frac{\tau}{(1 + 6D\tau/w^2)}\ln\left\{\left(1 + \frac{V^0}{V_C^0}\frac{\dot{V}_{c0}}{\dot{V}_L}\right)\left(1 + \frac{w^2}{6D\tau}\right)\exp\left(-\frac{6Dt_1}{w^2}\right) - \frac{w^2}{6D\tau}\right\} \qquad (16)$$

Note that this equation corrects an error in the final line of the derivation given in the appendix of Kirkland et al. [19] and is also more general in allowing t_1 to differ from τ. The corrected result for TDE programming of cross flow rate (for which $t_1 = \tau$) at constant outlet flow rate, as considered by Kirkland et al. [19], is given in the Electronic supplementary materials (ESM). For exponential decay of $\dot{V}_c$ and constant $\dot{V}_L$, Eq. 16 yields a good estimate of elution times for particles that are well retained but are also eluted well before the projected steric inversion. Equations 15 and 16 show how t_r is related to diffusion coefficient D, and therefore to particle hydrodynamic diameter or to molecular weight. It will be shown later that the determination of nonequilibrium

bandspreading under programmed flow conditions requires a numerical approach. The parallel determination of elution time using a more accurate calculation of $R(t)$, as described below, is recommended for exponential decay of cross flow rate and is necessary for other mathematical forms of programmed cross flow rate.

Numerical determination of retention time

As mentioned above, the retention ratio R, being a function of λ_0, and therefore of $\dot{V}_c$, is a function of time. It has long been known that the retention ratio in As-FlFFF deviates from that for symmetrical FlFFF due to the variation in cross flow velocity across the channel thickness [7]. The deviation is most significant for weakly retained sample components, and accurate determination of elution time should take this into account. The expression for retention ratio in As-FlFFF with correction for steric exclusion was recently presented [27]. ESM Table S1 shows numerically calculated values of R, the nonequilibrium parameter χ, and the product χR over a wide range of λ_0 from 0.0001 to 1024. The tabulated values do not include a steric exclusion correction. The incorporation of the steric exclusion correction into the calculation of R in As-FlFFF requires the integration of concentration profiles over the region of the channel thickness that is accessible to the particle or molecule centers. The core-channel approach taken by Giddings [26] to derive an expression for R in conventional FFF, where field-induced transverse velocity is constant across the channel, is not strictly valid for As-FlFFF. However, when particles or molecules are small in comparison to channel thickness, the errors associated with this approach are negligible while the savings in computation are considerable, which is particularly important for the modeling of programmed operation which requires repeated calculations at incrementally different conditions. The core-channel retention ratio R_c is calculated for the fraction of the channel thickness accessible to the particle or molecule centers. This region has a thickness of $(1 - 2\alpha)w$, and at the exclusion distance from the membrane, the transverse fluid velocity is $(1 - 3\alpha^2 + 2\alpha^3)|u_0|$ [7, 27]. The core-channel retention parameter λ_c is therefore given by $\lambda_0/((1 - 2\alpha)(1 - 3\alpha^2 + 2\alpha^3))$. Rather than numerically evaluating R_c for every λ_c corresponding to each interval in time and each interval in ϕ, it is far more efficient to use a cubic spline interpolation [35] from tabulated values such as those of ESM Table S1. The estimate of R is then obtained using the relationship [26]

$$R = 6\alpha(1-\alpha) + (1-2\alpha)^2 R_c \qquad (17)$$

ESM Figure S1 shows the error associated with the use of Eq. 17 for the relatively large values of α of 0.0005, 0.001, 0.002, and 0.005, corresponding to spherical particle

diameters of 0.25, 0.5, 1.0, and 2.5 μm for a channel thickness of 250 μm. In each case, R is underestimated with the maximum error given at λ_0 of about 0.075, corresponding to accurate R values of 0.415, 0.418, 0.423, and 0.439 and errors for Eq. 17 of 0.0203, 0.0403, 0.0792, and 0.188 %, respectively. Errors are even smaller for both smaller α and smaller λ_0. The large saving in computational time is therefore justified.

Local sample zone velocity is expressed as

$$\frac{dz}{dt} = R(t) \; \langle v(z,t) \rangle = \frac{R(t) \; \dot{V}(z,t)}{w b_z} \tag{18}$$

A rearrangement of Eq. 18 shows that

$$\delta z = \frac{R(t) \; \dot{V}(z,t)}{w b_z} \delta t \tag{19}$$

The distance δz migrated in the small time interval δt depends on both the time t and the position of the particles z. The migration of a monodisperse sample component may be followed by summing increments in δz from the focusing position to the outlet in order to determine its elution time. The time t at any point is simply the sum of the intervals δt so far considered, and the position z is the summation of the corresponding intervals δz from the initial position z'. Using a simple Euler approach, successive intervals may be calculated using the conditions at the previous position:

$$\delta z_{j+1} = \frac{R(t_j) \; \dot{V}(z_j, t_j)}{w b(z_j)} \delta t \tag{20}$$

where $t_j = j\delta t$ and $z_j = z' + \sum_{k=1}^{j} \delta z_k$, so that $t_0 = 0$, $z_0 = z'$, and $z_{j+1} = z_j + \delta z_{j+1}$. This approach first necessitates the calculation of the focusing point z'. The local volumetric flow rate is given by

$$\dot{V}(z_j, t_j) = \dot{V}(0, t_j) - \frac{\dot{V}_c(t_j) w}{V_C^0} \int_0^{z_j} b_z \; dz \tag{21}$$

or, alternatively, by

$$\dot{V}(z_j, t_j) = \dot{V}(L, t_j) + \dot{V}_c(t_j) \left(1 - \frac{w}{V_C^0} \int_0^{z_j} b_z dz \right) \tag{22}$$

where the appropriate channel breadth function b_z is used. Successive δz_j are summed until z_{j+1} just equals or exceeds L. Such an approach was followed by Nilsson et al. [36] for exponential decay of cross flow rate. A possible advantage of carrying out the summation in δz_j is that the shear rate at the membrane surface can be calculated for the center of mass of each zone as it migrates along the channel. This might be of interest if particle–membrane interactions are suspected to influence retention. For example, there may be some critical ratio of shear rate to flow velocity through the membrane below which the particles or molecules become immobilized. The influence of local conditions on the elution of a sample component zone is complicated by the variation of conditions across the breadth of the zone, however; part of the zone may be adversely affected while other parts are not.

If particle–membrane interactions are not an issue, an alternative approach to that considered above is possible. The rate that channel volume is swept through by the position of the center of mass of the sample zone may be considered:

$$\frac{dV}{dt} = R(t) \; \dot{V}(V,t) \tag{23}$$

Successive intervals in channel volume passed through in time intervals δt can be calculated using an equation analogous to Eq. 20:

$$\delta V_{j+1} = R(t_j) \; \dot{V}(V_j, t_j) \delta t \tag{24}$$

where local channel volumetric flow rate is written as a function of V_j, the volume of the channel from the inlet to the local position, and discrete time t_j. Following Eq. 7, it is apparent that

$$\dot{V}(V_j, t_j) = \dot{V}(0, t_j) - \dot{V}_c(t_j) \frac{V_j}{V_C^0}$$

$$= \dot{V}(L, t_j) + \dot{V}_c(t_j) \left(1 - \frac{V_j}{V_C^0} \right) \tag{25}$$

The current V_j is obtained via the summation of previous increments to channel volume

$$V_j = V_C^0 - V^0 + \sum_{k=1}^{j} \delta V_k \tag{26}$$

where the channel volume up to the initial point V_0 is given by $V_0 = V_C^0 - V^0$, and it is not necessary to determine z'. It also follows that $V_{j+1} = V_j + \delta V_{j+1}$. Equation 24 can now be written in the form

$$\delta V_{j+1} = R(t_j) \left(\dot{V}(0, t_j) - \frac{\dot{V}_c(t_j)}{V_C^0} \left(V_C^0 - V^0 + \sum_{k=1}^{j} \delta V_k \right) \right) \delta t \tag{27}$$

or, alternatively, in the form

$$\delta V_{j+1} = R(t_j) \left(\dot{V}(L, t_j) + \frac{\dot{V}_c(t_j)}{V_C^0} \left(V^0 - \sum_{k=1}^{j} \delta V_k \right) \right) \delta t \tag{28}$$

The summation of successive δV_j is carried out until V_{j+1} just equals or exceeds V_C^0. The number of required intervals δt then indicates the elution time (of course, the final interval will

invariably be some fraction of δt consistent with the final increment to channel volume necessary to exactly obtain V_C^0). For these numerical calculations, $\dot{V}_c(t_j)$, which also influences $R(t_j)$, can follow any smooth mathematical function of time, or it can be a discontinuous function or series of functions, or indeed have an arbitrary variation with time. It is apparent from Eqs. 27 and 28 that, for any variation of $\dot{V}_c$ with time, provided non-idealities are insignificant and the elution adheres to the expression used for the retention ratio, the increments to channel volume are independent of the breadth profile of the channel. This means that, provided the retention ratio is not influenced by local channel flow velocity, elution times will also be independent of the channel breadth profile.

The equations and discussion above imply that a simple application of Euler's method may be used for summation of δz_j or δV_j. In practice, to better represent the gradually changing conditions across the intervals, a fourth-order Runge–Kutta summation may be carried out (see [37]). This involves the consideration of conditions at half time intervals. In fact, Nilsson et al. [36] used a similar approach. For the small time intervals typically considered, the improvement is modest, and very often negligible.

It is important to emphasize that Eqs. 27 and 28 are perfectly general. The values for $\dot{V}_c(t_j)$ and either $\dot{V}(0, t_j)$ or $\dot{V}(L, t_j)$ may correspond to a defined set of programmed conditions, or they may be quantities that are experimentally monitored during a sample analysis. The monitoring of flow rates can account for deviation from nominal set conditions or for flow rates that are arbitrarily varied as opposed to following precise functions of time. In any case, the mean elution time may be determined for any assumed ϕ, provided it is known how D and α are related to ϕ. The calculation of elution times for a series of discrete ϕ allows the use of interpolation to associate a value of ϕ_i to every discrete elution time t_i. This is the basis of the integral approach to FFF data reduction (transformation of fractogram to size or molecular weight distribution) [38]. The approach is here shown to be applicable to As-FlFFF.

Bandspreading

As a monodisperse zone passes along the channel, its breadth is influenced by the loss of carrier solution through the membrane and by the changing channel breadth. It was explained in part I [25] that the loss of carrier solution tends to reduce the zone breadth while the reduction in channel breadth tends to increase the zone breadth. For the calculation of the contributions to bandspreading, the channel may be considered to be divided

into a series of small intervals, with each contributing to the breadth of the zone as it migrates through it. The conditions across the breadth of a zone can vary significantly, but it was explained in part I [25] that a projected standard deviation in breadth of the zone can be considered as corresponding to the standard deviation expected when conditions at the center of mass are assumed to apply across the full zone. Then as the center of mass passes from one interval to the next, the zone variance must be adjusted for the changing volumetric flow rate and channel breadth before the next contribution to variance is added. In the case of programmed operation, this adjustment must take into account the change in flow rates with time as well as position. The variance in zone breadth σ_z^2 for center of mass at position and time (z_{i-1}, t_{i-1}) must therefore be adjusted by the ratio $(b_{i-1} \dot{V}(z_i, t_i)/b_i \dot{V}(z_{i-1}, t_{i-1}))^2$, or equivalently $(\langle v(z_i, t_i)\rangle/\langle v(z_{i-1}, t_{i-1})\rangle)^2$, as the center of mass passes to (z_i, t_i), where the next contribution $\delta\sigma_{z,i}^2$ is added. The summation of successive contributions to variance can be written as

$$\sigma_{z,i}^2 = \sum_{j=1}^{i} {}_c\delta\sigma_{z,j}^2 = \delta\sigma_{z,i}^2 + \left(\frac{\langle v(z_i, t_i)\rangle}{\langle v(z_{i-1}, t_{i-1})\rangle}\right)^2 \sum_{j=1}^{i-1} {}_c\delta\sigma_{z,j}^2 \quad (29)$$

where the subscript C on the summation signs indicates that they do not represent simple summations but mean velocity-corrected summations. In the same way as shown in part I [25] for isocratic operation, the expansion of successive terms in Eq. 29 shows that the mean velocity-corrected summation reduces to the simple summation:

$$\sigma_{z,i}^2 = \langle v(z_i, t_i)\rangle^2 \sum_{j=1}^{i} \frac{\delta\sigma_{z,j}^2}{\langle v(z_j, t_j)\rangle^2} \quad (30)$$

The variances represented in Eqs. 29 and 30 correspond to the projected variances where the conditions at the center of mass are imagined to extend across the whole breadth of the zone. As mentioned above, the conditions can vary significantly across a zone, distorting the distribution along the length or volume of the channel. The contributions to variance in the time of elution may alternatively be considered, but they are not simply summed as in isocratic operation, however; the change of retention ratio from interval to interval must be taken into account. An increase in R, as seen under programmed decay of cross flow rate, will reduce the variance in elution time simply because the zone velocity increases. Every fraction of the zone is influenced simultaneously by an instantaneous change in R. The progress of the center of mass of the zone in the time domain may be considered and the variance in elution time adjusted for the change in R from

the previous interval to the current before adding the current contribution:

$$\sigma_{t,i}{}^2 = \sum_{j=1}^{i} {}_C\delta\sigma_{t,j}{}^2 = \delta\sigma_{t,i}{}^2 + \left(\frac{R(t_{i-1})}{R(t_i)}\right)^2 \sum_{j=1}^{i-1} {}_C\delta\sigma_{t,j}{}^2 \quad (31)$$

The subscript C on the summation signs again indicates that they are not simple summations. By expanding successive terms, this may be shown to be equivalent to the simple summation given by

$$\sigma_{t,i}{}^2 = \frac{1}{R(t_i)^2} \sum_{j=1}^{i} R(t_j)^2 \delta\sigma_{t,j}{}^2 \quad (32)$$

The comments made with regard to the calculation of elution times using Eq. 27 or Eq. 28 are equally applicable to the calculation of σ_t^2 using Eq. 32. If $\delta\sigma_{t,j}{}^2$ may be calculated for local conditions for a zone migrating along the channel, then the zone variance in elution time may be predicted for any given variation in channel and cross flow rates. This allows the calculation of F_ϕ (by interpolation) for every discrete elution time t_i and corresponding ϕ_i. The integral approach to FFF data reduction [38] not only performs the transformation of the fractogram to a size or molecular weight distribution, it also provides the important knowledge of F_ϕ across the distribution.

Nonequilibrium bandspreading

As for the retention ratio, the core-channel approach can be taken to obtain the nonequilibrium bandspreading parameter χ in order to save computational time. The core-channel λ_c is calculated as before. The core-channel value of the product $R_c\chi_c$ can then be efficiently obtained using cubic spline interpolation of the tabulated data (ESM Table S1) and the product $R\chi$ calculated via the relationship [14, 26]

$$R\chi = R_c\chi_c(1-2\alpha)^6 \quad (33)$$

ESM Figure S1 shows the error associated with this approach, again for the examples of α of 0.0005, 0.001, 0.002, and 0.005. Equation 33 slightly underestimates the correct value, with maximum error occurring at λ_0 of about 0.045. A λ_0 of 0.045 corresponds to R values of 0.256, 0.259, 0.265, and 0.281, and the errors given by Eq. 33 are 0.105, 0.210, 0.417, and 1.028 %, respectively. For both smaller α and stronger retention, the errors are smaller, justifying the approach. The savings in computational time are considerable

for calculations related to programmed cross flow rate conditions.

The local nonequilibrium plate height is given by [29]

$$H_{neq}(z_j, t_j) = \frac{w^2}{D} \chi(t_j) \langle v(z_j, t_j) \rangle \quad (34)$$

where χ is the nonequilibrium parameter that is a function of λ_0, and therefore of time, and of α when the steric exclusion correction is included [26, 27, 30]. The local contribution to zone variance on migrating a small distance δz is then given by

$$\delta\sigma_{z,j}{}^2 = H_{neq}(z_j, t_j) \ \delta z = \frac{w^2}{D} \chi(t_j) \langle v(z_j, t_j) \rangle \ \delta z \quad (35)$$

Local zone velocity is given by

$$\frac{\delta z}{\delta t} = R(t_j) \langle v(z_j, t_j) \rangle \quad (36)$$

and therefore

$$\delta\sigma_{z,j}{}^2 = \frac{w^2}{D} \chi(t_j) R(t_j) \langle v(z_j, t_j) \rangle^2 \delta t \quad (37)$$

This can be converted to an increment in variance of retention time by dividing by the square of the local zone velocity $R(t_j)^2 \langle v(z_j, t_j) \rangle^2$

$$\delta\sigma_{t,j}{}^2 = \frac{w^2}{D} \frac{\chi(t_j)}{R(t_j)} \delta t \quad (38)$$

Summing the contributions to variance in retention time according to Eq. 32 shows that

$$\sigma_{t,i}{}^2 = \frac{w^2}{DR(t_i)^2} \sum_{j=1}^{i} \chi(t_j) R(t_j) \delta t \quad (39)$$

Suppose that $t_r = (i + f)\delta t$, where f is the final fraction of a time interval δt required for the center of mass to reach the channel outlet, then

$$\sigma_{t,neq}{}^2 = \frac{w^2 \delta t}{D \ R(t_r)^2} \sum_{j=1}^{i+f} \chi(t_j) R(t_j) \quad (40)$$

The calculation of elution time and variance in elution time due to nonequilibrium bandspreading may therefore be calculated by summations over small time intervals δt without specifying a channel breadth profile. They are in fact independent of the channel breadth profile. In practice, the summation represented by Eq. 40 is carried out using Simpson's 1/3 rule, taking values of the product of χ and R at j and $j + 0.5$ intervals. Again, the improvement over a simple interval summation is generally modest for small time intervals.

Multipath bandspreading

It was explained in part I [25] how slight unevenness in the membrane surface and small variations in membrane permeability must contribute to bandspreading. Different fractions of the sample follow different paths along the channel having different mean fluid velocities and different mean transverse fluid velocities through the membrane. The fractions consequently reach the channel outlet at slightly different times, thereby contributing to bandspreading. Under isocratic conditions, this multipath contribution is not expected to be a strong function of retention ratio as the relative variation in mean fluid velocity and relative variation in retention ratio should be similar for all components. There should not be a significant change in the multipath effect with change of cross flow rate as the fractions of a component following different paths should show the same relative change in R. It is possible that the membrane may be forced into better contact with the supporting frit at high cross flow rate, but this supposes that the membrane draws away from the frit at a low cross flow rate, which would result in very poor efficiency or even split peaks. This possibility will therefore be discounted, and it will be assumed that the membrane remains in good contact with the frit at all cross flow rates.

It was also pointed out in part I [25] that the scale of the multipath effect in As-FlFFF as well as its two-dimensional nature do not allow lateral diffusional exchange of material between streams, as may occur in packed bed chromatographic columns [39]. The flow pattern along the channel can be assumed to be fixed and independent of the channel and cross flow rates. The multipath bandspreading is therefore the result of the distribution of sample across several independent streams having slightly different mean channel flow velocities and slightly different mean cross flow velocities, the relative differences between streams remaining constant under programmed conditions. To model the contribution to multipath bandspreading under programmed conditions, it will also be assumed that the relative differences in mean velocities and membrane permeabilities between different paths are fairly constant along the channel length. It is not necessary to make this assumption for isocratic conditions.

Consider a path for which the elution time for a monodisperse material is one standard deviation $\sigma_{t,m}$ lower than the mean elution time t_r. The difference is due to the fact that, for this elution path, the increments δV_{j+1} are attained in slightly less time than would material eluting at the mean migration rate from the same V_j and t_j, in time intervals of $(1-\varepsilon)\delta t$, where ε is a small positive correction factor. Therefore, δV_{j+1} is calculated using Eq. 24 or its equivalent, but the cumulative elution time is incremented by $(1-\varepsilon)\delta t$.

For the special case of isocratic elution, this gives the simple result

$$t_r - \sigma_{t,m} = (1-\varepsilon)t_r \tag{41}$$

For isocratic elution, the limiting multipath plate number N_m has been defined as $(t_r/\sigma_{t,m})^2$ [25], and it follows from Eq. 41 that $\varepsilon = 1/\sqrt{N_m}$. For $N_m = 3000$, for example, $\varepsilon = 0.0183$. It is now apparent that $\sigma_{t,m}$ may be obtained for any sample component eluting under programmed conditions by first solving for t_r and then for $t_r - \sigma_{t,m}$ by applying the multiplicative factor $(1-\varepsilon) = (1 - N_m^{-0.5})$ to successive δt, with δV_{j+1} as calculated using Eq. 24 or its equivalent. The value for N_m depends on each assembled channel and membrane and can be determined experimentally as explained in the ESM of part I [25]. It may be found in practice that N_m varies to some extent with particle size, molecular weight, or flow conditions. Such variation could be taken into account, but for the purposes of this work, N_m will be assumed to be constant.

Other contributions to bandspreading

Other contributions are relatively minor or can be made minor by suitable selection of conditions, as in isocratic operation. These are discussed in the ESM.

Comparison of programmed and isocratic elution

Typical parameters of channel thickness $w = 0.025$ cm, channel volume $V_C^0 = 0.75$ mL, carrier fluid viscosity $\eta = 0.01$ P, and temperature $T = 298$ K were assumed, together with Boltzmann constant $k = 1.38065 \times 10^{-23}$ J/K. A polydisperse nanoparticle sample was assumed to be initially focused at the inlet (so that $V^0 = V_C^0$). This initial position was also considered in part I [25], where it was explained that focusing of the sample at some other position could have been considered, but this would not have contributed to the discussion. The nanoparticles were assumed to be spherical so that a simple steric exclusion correction could be taken into account. To show the influence of F_d on the outlet polydispersity (see the next section), two sets of conditions involving exponential decay of cross flow rate were considered. Condition I corresponds to an initial cross flow rate $\dot{V}_{c0} = 2.0$ mL/min, constant outlet flow rate $\dot{V}_L = 0.2$ mL/min, pre-decay time $t_1 = 1.0$ min, and exponential time constant $\tau = 5.0$ min. Condition II corresponds to $\dot{V}_{c0} = 6.0$ mL/min, $\dot{V}_L = 0.6$ mL/min, and the same time constants. These conditions were selected to obtain almost identical elution times (see approximate Eq. 16, valid for $\alpha << \lambda_0 << 1$), and therefore selectivity, but different levels of F_d. In each case, a multipath bandspreading equivalent to a limiting plate number N_m of 3000 under isocratic conditions was assumed.

Figure 1 shows the predicted F_d as a function of d (on a log scale) for programmed condition I (full black curve). Also included for comparison are the predicted F_d curves for isocratic elution at $\dot{V}_c$ values of 2.0, 1.0, 0.5, and 0.25 mL/min, with $\dot{V}_L$ held at 0.2 mL/min (full red, green, blue, and purple curves, respectively). All full curves were calculated using the equations for R and χR for As-FlFFF taking the core-channel approximation for steric exclusion as explained above. (It should be pointed out that the lower limit on particle size for retention and fractionation is ultimately determined by the membrane size cutoff. Particles smaller than the cutoff will not be retained in the channel by the membrane and will be lost. This aspect is not specifically considered in this work as the focus is on illustrating the predictions made by the equations derived to model the system.)

For condition I, a maximum F_d of 1.98 is predicted for $d = 0.0094$ μm. For d values of 0.001, 0.01, and 0.1 μm, F_d is predicted to be 0.545, 1.98, and 0.490, respectively. For comparison, the dashed curves were calculated using the equations for conventional FFF in which field-induced transverse velocity is constant across the channel thickness. These equations are valid for Sym-FlFFF where the transverse fluid velocity component is assumed to be constant across the thickness. These equations are therefore referred to as the Sym-FlFFF equations in the following discussion. For the programmed condition I, the Sym-FlFFF equations result in a slightly higher predicted F_d than the As-FlFFF equations across the full diameter range. A slightly higher F_d for smaller diameters (weak retention) is predicted for isocratic conditions. Under the programmed condition I, the F_d values predicted using the Sym-FlFFF equations were 34, 14, and 27 % higher at d values of 0.001, 0.01, and 0.1 μm, respectively, which is quite significant.

For programmed condition I, the projected steric inversion diameter $d_i > 1.0$ μm, whereas under the different isocratic conditions, the projected d_i (where F_d falls to zero) values are smaller than 1.0 μm and inversely related to $\dot{V}_c^{0.5}$ (see Eq. 32 of part I [25], valid for isocratic conditions). The F_d for isocratic elution may be much higher over some limited range of d than for programmed conditions, but the range of diameters eluted in the normal mode is reduced. For example, isocratic elution at $\dot{V}_c$ of 2.0 mL/min shows no loss of F_d at low d, a much higher maximum F_d of 11.4 at 0.058 μm, but a projected d_i of about 0.28 μm. Isocratic elution at a lower cross flow rate predicts higher projected d_i, but considerably lower F_d for the smaller particle diameters.

The elution times for the larger d are greatly reduced by the programmed decay of cross flow rate, which is, of course, one of the objectives of programming. ESM Figure S2 shows the predicted elution times as functions of log d for the same set of programmed and isocratic conditions. The maxima in the isocratic curves correspond to the projected inversion diameters. The differences between the elution times predicted using the As-FlFFF and Sym-FlFFF equations are too small to distinguish on the scale of the time axis, and only a single set of curves is included in the figure. Relative differences are significant, however.

Figure 2 shows the variation of selectivity S_d with log d for the different conditions. In isocratic operation, S_d approaches but does not quite attain a level of unity and remains fairly constant until steric effects start to influence elution and S_d begins to fall, approaching zero at the projected d_i. The range of d where S_d is close to unity moves to higher diameters as $\dot{V}_c$ is reduced, and the range is also reduced to some degree. In part I [25], an approximate equation for S_d for isocratic operation was presented which is valid for the range of d where $\lambda_0 << 1$ and $\alpha << 1$; it is not

Fig. 1 Fractionating power F_d as a function of d (log scale) for programmed condition I (*black curves*) and isocratic conditions with $\dot{V}_c$ values of 2.0, 1.0, 0.5, and 0.25 mL/min (*red*, *green*, *blue*, and *purple curves*, and as labeled) and $\dot{V}_L = 0.2$ mL/min in all cases. *Full curves* calculated using As-FlFFF equations and *dashed curves* using Sym-FlFFF equations
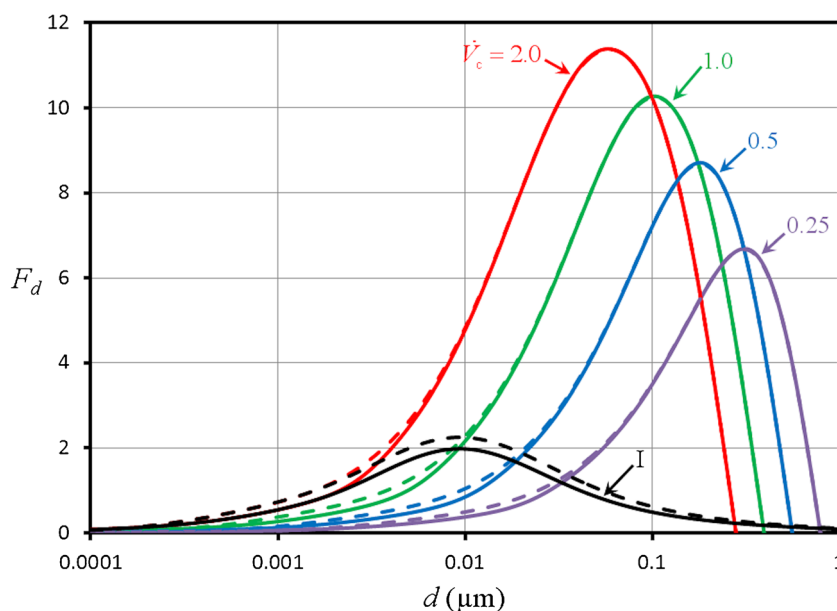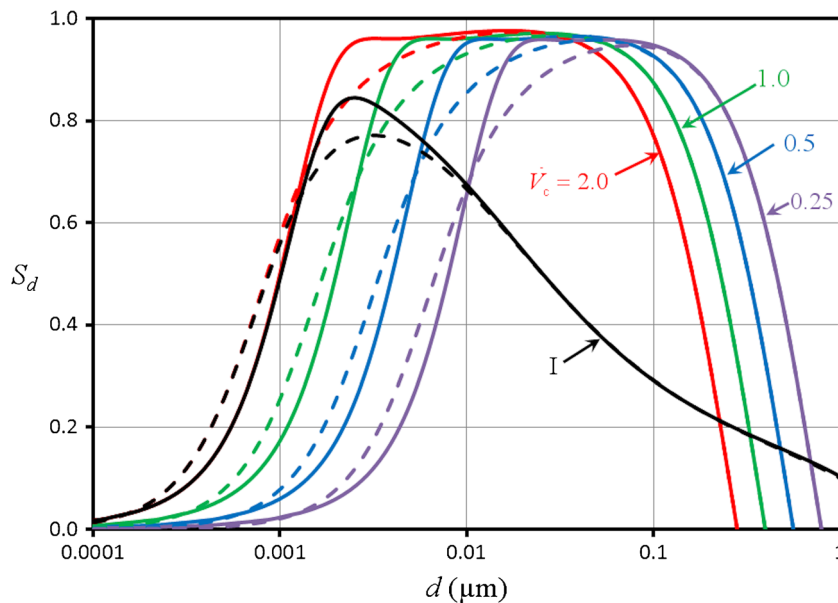
Fig. 2 Selectivity S_d as a function of d (log scale) for programmed condition I (*black curves*) and isocratic conditions as given in the caption to Fig. 1. *Full curves* calculated using As-FlFFF equations and *dashed curves* using Sym-FlFFF equations

valid for the range of d over which S_d rises to the plateau. The plateau is attained when λ_0 falls to about 0.07 in As-FlFFF, corresponding to $R = 0.387$ (results for S_M were plotted on a linear scale in M in Fig. S1 of the ESM of part I [25], where this rise to the plateau was not made evident). Under the programmed condition I, S_d is predicted to rise over the region of d where λ_0 decreases toward 0.07 and then to fall steadily over a wide range of d as $\dot{V}_c$ decays. This shows the desired effect of programmed decay of cross flow rate on selectivity mentioned in the introduction and reflects the reduced elution times predicted for the larger particles. Note that S_d does not rise to the level attained for isocratic conditions with $\dot{V}_c = 2.0$ mL/min before falling. This is because the cross flow rate starts to decay at $t_1 = 1.0$ min, which is very close to the void time of 0.899 min. Those particles for which $\lambda_0 = 0.07$ at $\dot{V}_c = 2.0$ mL/min are eluted after the start of the cross flow decay. In Fig. 2, the full curves were again predicted using the As-FlFFF equations, and the dashed curves the Sym-FlFFF equations. Note that the rise of S_d to the plateau for isocratic operation is not so abrupt for the Sym-FlFFF equations, and the range of d for each plateau is consequently reduced. This is also true in the case of programmed operation, but the solutions for Sym-FlFFF and As-FlFFF equations converge as $\dot{V}_c$ decays. The differences in predicted S_d are a consequence of the slightly different dependence of asymmetrical R_{As} and symmetrical R_{Sym} on λ_0. For FlFFF of spherical nanoparticles where $\lambda_0 \propto 1/d$, it can be shown from Eq. 3 that

$$S_d = \frac{\lambda_0}{R} \frac{dR}{d\lambda_0} \tag{42}$$

It is also interesting to compare the predicted contributions to bandspreading as functions of d for the different conditions. Figure 3 shows the nonequilibrium contribution $\sigma_{t,neq}$ as a

function of $\log d$ for programmed condition I and the same isocratic conditions. In the case of isocratic elution, the non-equilibrium contribution rises to a relatively constant level before decreasing as the projected steric inversion is approached. This is as expected and is consistent with the approximate Eq. 36 of part I [25]. For the assumptions made here, this may be written as

$$\sigma_{t,neq} = \frac{V_C^0}{V_c} \left(\frac{2}{3} \ln \left(\frac{\dot{V}_c}{V_L} + 1 \right) \right)^{0.5} \left(1 + f^2 \right)^{-1.5} \tag{43}$$

in which f is the ratio of d to the projected d_i. Consistent with Eq. 43, the level of each plateau in $\sigma_{t,neq}$ increases with reduction of $\dot{V}_c$. The final factor in Eq. 43 involving f accounts for the roll-off in $\sigma_{t,neq}$ from each plateau toward d_i and beyond. In Fig. 3, the full curves were predicted using the equations for As-FlFFF and the dashed curves using the Sym-FlFFF equations. The As-FlFFF equations predict a steeper climb and some overshoot before reaching the plateau in $\sigma_{t,neq}$, while the Sym-FlFFF equations predict a more gradual rise. There is therefore a significant difference in behavior in the lower region of the plateau. Under programmed condition I, $\sigma_{t,neq}$ increases with d for the range plotted, and the Sym-FlFFF equations predict a considerably lower contribution to bandspreading than the As-FlFFF equations. For example, the Sym-FlFFF equations predict 6.6, 12, 20, and 21 % lower $\sigma_{t,neq}$ at d values of 0.001, 0.01, 0.1, and 1.0 μm, respectively.

Figure 4 shows the multipath contributions $\sigma_{t,m}$ as functions of $\log d$. Under isocratic conditions, $\sigma_{t,m}$ is seen to increase with d, rising to some maximum at the steric inversion point before falling again. Of course, under isocratic conditions it is assumed that $\sigma_{t,m} = t_r / \sqrt{N_m}$ and in the region before inversion, and $\sigma_{t,m}$ is expected to increase with t_r and

Fig. 3 Predicted nonequilibrium contribution to bandspreading $\sigma_{t,neq}$ as a function of d (log scale) for programmed condition I (*black curves*) and isocratic conditions as given in the caption to Fig. 1. *Full curves* calculated using equations for As-FlFFF and *dashed curves* using Sym-FlFFF equations
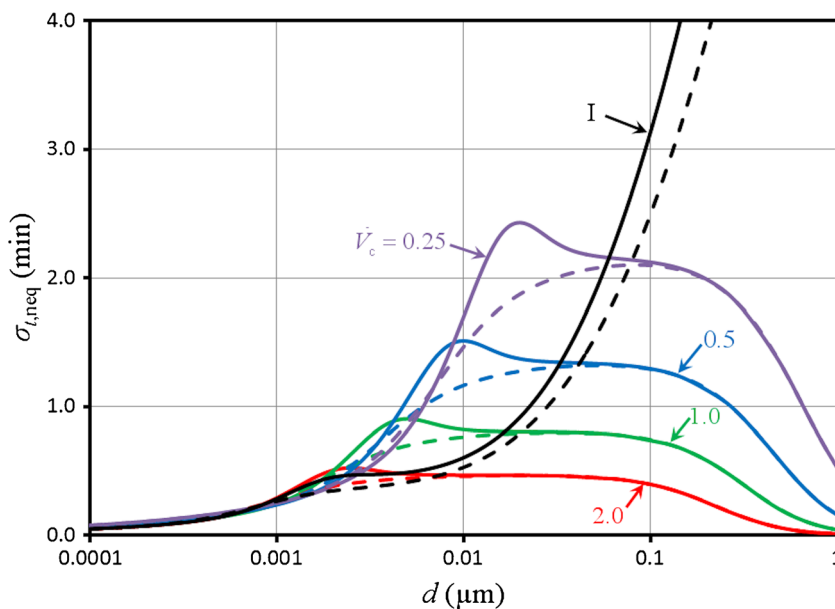
therefore with $\dot{V}_c$. Programmed condition I is predicted to give a relatively small contribution to $\sigma_{t,m}$ across the full range of d plotted; multipath bandspreading is therefore suppressed under programmed conditions. Equation 8 may be modified to take into account the $(1-\varepsilon)$ factor for δt, as shown in ESM Eq. S2. This may then be solved for the case of exponential decay of $\dot{V}_c$, constant $\dot{V}_L$, and the $R \approx 6\lambda_0$ approximation to obtain an approximate solution for $t_r - \sigma_{t,m}$ in the form of Eq. 16. The result, valid for $\alpha << \lambda_0 << 1$, is shown in ESM Eq. S3. It is also pointed out in the ESM that a crude estimate of $\sigma_{t,m} \approx \tau \ln(1/(1-\varepsilon))$ is obtained when $D\tau/w^2 \rightarrow 0$, and α remains negligible. For condition I, approximate $\sigma_{t,m}$ values of 0.100 and 0.093 min are obtained using Eqs. 16 and S3 for d values of 0.01 and 0.1 μm, respectively. These compare with

the values obtained numerically, and as plotted in Fig. 4, of 0.092 and 0.122 min, respectively, and the $\sigma_{t,m} \approx \tau \ln(1/(1-\varepsilon))$ estimate of 0.092 min. As expected, there is no observable difference between predictions of $\sigma_{t,m}$ based on the As-FlFFF and Sym-FlFFF equations on the scale of the $\sigma_{t,m}$ axis, and only one set of curves is included in the figure. Relative differences are significant at low retention, however. Finally, Fig. 5 shows the results of summing the contributions to variance due to nonequilibrium and multipath effects for the different conditions. Again, full curves correspond to As-FlFFF equations and dashed curves to Sym-FlFFF equations.

The results for programmed condition II are shown in ESM Figs. S3 to S8, and they are also briefly discussed in the ESM. In these figures, the programmed condition II is compared

Fig. 4 Predicted multipath contribution to bandspreading $\sigma_{t,m}$ as a function of d (log scale) for programmed condition I (*black curve*) and isocratic conditions as given in the caption to Fig. 1. The curves calculated using As-FlFFF and Sym-FlFFF equations are indistinguishable on the scale of the $\sigma_{t,m}$ axis, as mentioned in the text
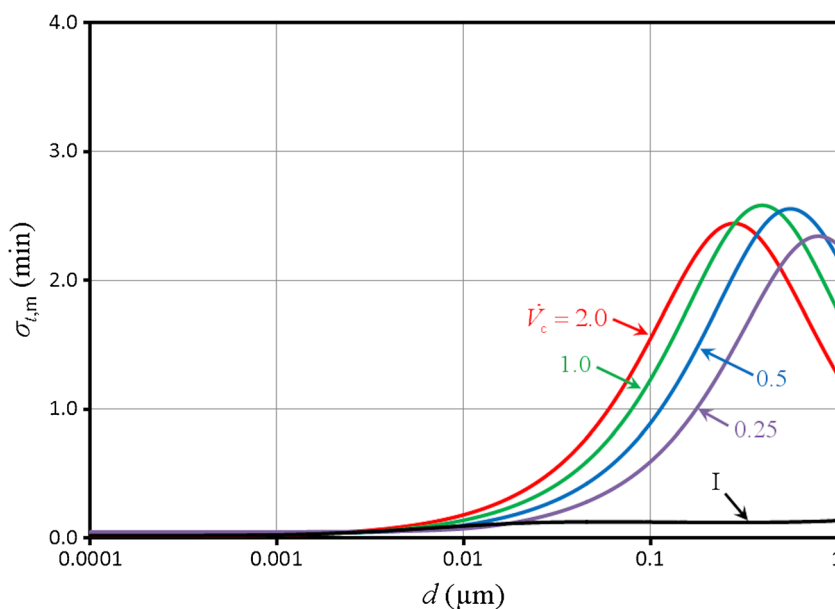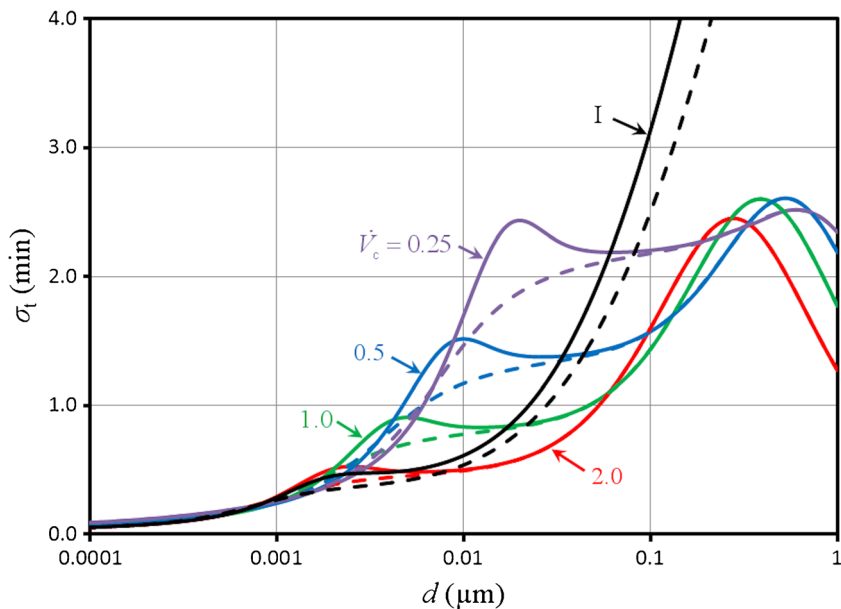
Fig. 5 Predicted σ_t, calculated by summing the contributions to variance due to nonequilibrium and multipath effects, as functions of d (log scale) for programmed condition I (*black curves*) and isocratic conditions as given in the caption to Fig. 1. *Full curves* calculated using As-FlFFF equations and *dashed curves* using Sym-FlFFF equations

with isocratic elution with $\dot{V}_c$ values of 6.0, 3.0, 1.5, and 0.75 mL/min and $\dot{V}_L = 0.6$ mL/min. The maximum F_d for condition II is predicted to be 5.81, almost three times higher than for condition I, and at the same particle diameter $d = 0.0094$ μm as for condition I. For d values of 0.001, 0.01, and 0.1 μm, F_d values were predicted to be 1.43, 5.80, and 1.61, respectively. At this higher level of F_d, the Sym-FlFFF equations for predicting F_d do not deviate so strongly from the As-FlFFF equations. The Sym-FlFFF equations predict F_d values just 18, 1, and 3 % higher than the As-FlFFF equations at d values of 0.001, 0.01, and 0.1 μm, respectively. While the predicted F_d is almost three times higher for programmed condition II than for condition I, the elution times are very similar when the steric perturbation remains small. The elution times for conditions I and II are within 5 % of one another for d between 0.002 and 0.4 μm. This is as expected and is consistent with Eq. 16. For smaller particles, the difference is greater because initial void times differ, and for larger particles, the difference increases because of the lower projected d_i for condition II. The elution times for the isocratic conditions shown in Figs. S2 and S4 (see ESM) are also very similar when $\alpha << \lambda_0$. This is because both the void times and the values of λ_0 for the conditions shown in ESM Fig. S4 are one third of those for the respective conditions of ESM Fig. S2. Their influence on t_r therefore approximately cancels when $\alpha << \lambda_0$.

Relation of fractionating power to channel outlet polydispersity

The method of predicting outlet polydispersity for any given set of experimental conditions was explained in part I [25]. It is

based on the approach taken by Schure [40]. A log-normal number distribution in particle diameter was assumed for the sample with number average diameter $\overline{d}_n$ of 0.01 μm and standard deviation σ_d of 0.0075 μm. The normalized number distribution is given by

$$N(d) = \frac{1}{\sqrt{2\pi}d\sigma} \exp\left(-\frac{(\ln d - \mu)^2}{2\sigma^2}\right) \tag{44}$$

in which

$$\mu = \ln\left(\frac{\overline{d}_n}{\left(1 + (\sigma_d/\overline{d}_n)^2\right)^{0.5}}\right) \tag{45}$$

and

$$\sigma = \left(\ln\left(1 + (\sigma_d/\overline{d}_n)^2\right)\right)^{0.5} \tag{46}$$

For each of the programmed conditions I and II described earlier, a retention time–particle diameter matrix was set up with 10,000 equal intervals in diameter up to 0.5 μm (so that $\delta d = 5 \times 10^{-5}$ μm) across the horizontal and 1740 equal intervals in time up to 21.75 min ($\delta t = 0.0125$ min) in the vertical direction. For each discrete d, a Gaussian elution curve was assumed with mean elution time given by summing contributions to channel volume given by Eq. 28 until the outlet is reached and standard deviation in elution time calculated by summing contributions to variance due to nonequilibrium and multipath contributions. The Gaussian was weighted by the diameter number distribution function and put into the respective column of the matrix. The number distribution in particle
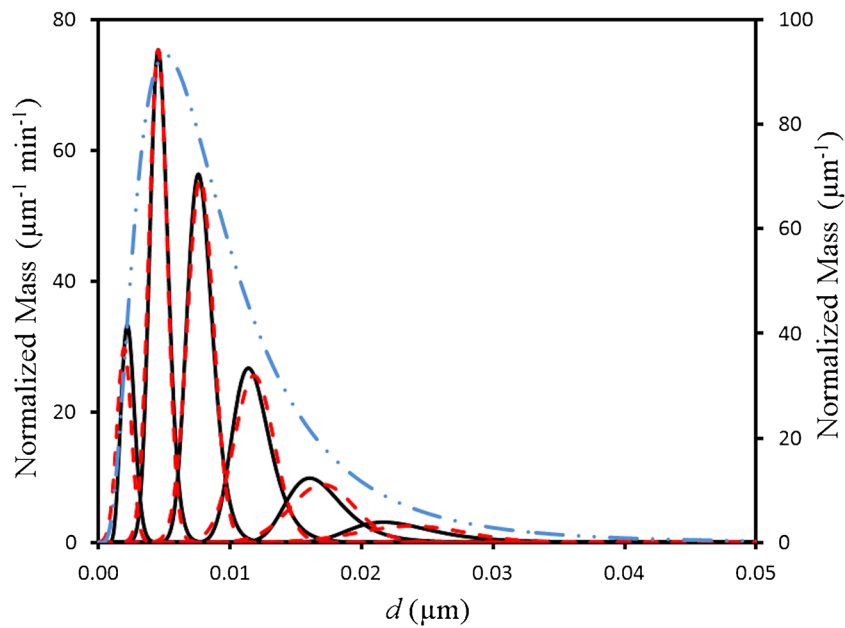
Fig. 6 Predicted outlet particle diameter number distributions at 2, 4, 6, 8, 10, and 12 min for programmed condition I for a sample having a log-normal number distribution in particle diameter with $\bar{d}_n = 0.01$ μm and $\sigma_d = 0.0075$ μm. Nonequilibrium bandspreading and multipath bandspreading consistent with a limiting overall system efficiency of 3000 plates under isocratic conditions were taken into account. *Full black curves* correspond to data in respective rows of the t_r–d matrix. *Dashed red curves* correspond to Gaussians with mean d corresponding to monodisperse d predicted to elute at respective t_r and σ_d corresponding to apparent $\sigma_{d,app}$ calculated using Eq. 47. *Dash-dotted blue curve* shows the sample particle diameter number distribution referring to the *right-hand axis*

size eluting at any discrete time is then given by the values across the row corresponding to that time.

Figure 6 shows the predicted outlet number distributions in particle diameter at elution times of 2, 4, 6, 8, 10, and 12 min for the fractionation of the log-normal sample (full black curves) under programmed condition I as determined using the time–diameter matrix. The normalized log-normal distribution assumed for the sample is also shown as a dash-dotted blue curve, referring to the right-hand axis. Also included are what Schure [40] referred to as the predicted apparent number distributions calculated as Gaussians with standard deviations in particle diameter given by

$$\sigma_{d,app} = \frac{\sigma_t}{dt_r/dd} = \frac{d}{4F_d} \quad (47)$$

Fig. 7 Predicted F_d (*full curves*) and S_d (*dashed curves, right-hand axis*) as functions of d (log scale) for programmed conditions I and II (*red* and *black curves, respectively*)
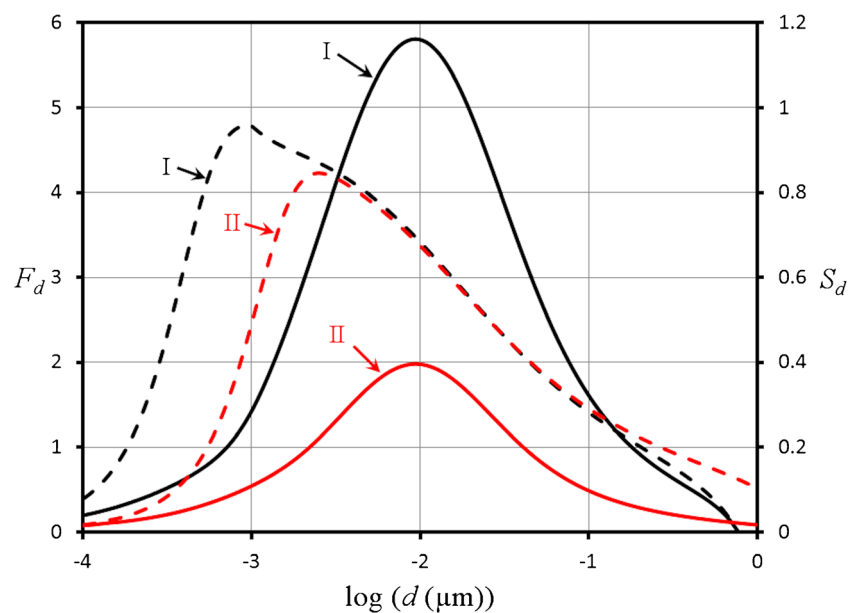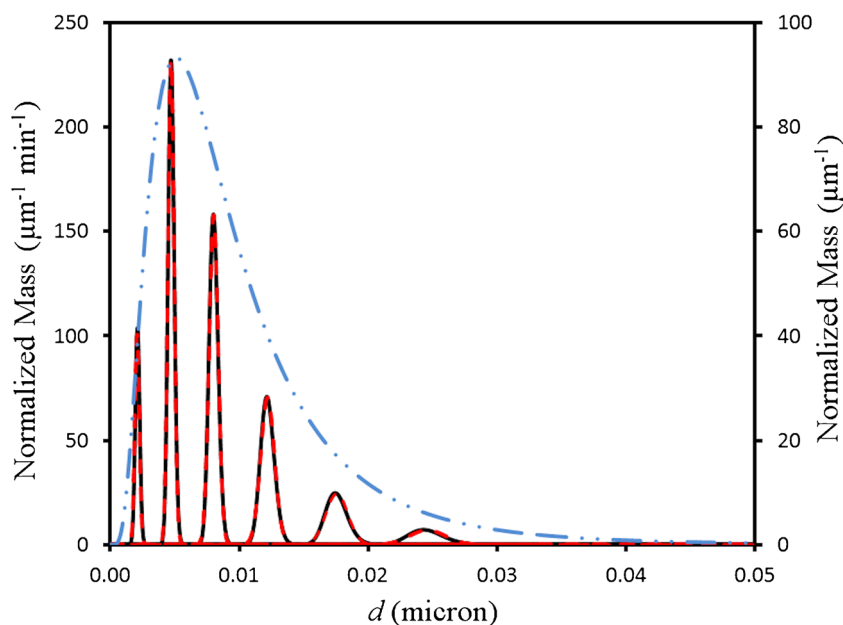
Fig. 8 Predicted outlet particle diameter number distributions at 2, 4, 6, 8, 10, and 12 min for programmed condition II for the same log-normal sample considered for Fig. 6. Remaining details correspond to the caption for Fig. 6


with d corresponding to the monodisperse particle diameters predicted to elute at mean elution times of 2, 4, 6, 8, 10, and 12 min. The latter are plotted as dashed red curves.

There is fairly good agreement between the two sets of distribution curves for all but the lowest elution time of 2 min. The poorer agreement at 2 min is attributable to two factors: (1) the F_d is low (0.917) at this time so that the relative polydispersity is high, and (2) the diameter d coincides with the steep front of the sample size distribution. The number distribution obtained from the row of the time–diameter matrix corresponding to 2 min will therefore be correctly skewed toward the sample distribution maximum. The predicted apparent number distribution (dashed red curve) is a

symmetrical Gaussian and cannot account for this effect. This effect leads to a discrepancy of almost 14 % between the monodisperse particle diameter predicted to elute at a mean t_r of 2 min and the $\overline{d}_n$ predicted at an elution time of 2 min. The approximation to σ_d as calculated using Eq. 47 is also 8 % in error. The skewing of the outlet distributions at 8, 10, and 12 min is also apparent in Fig. 6, although consequent errors are far less significant. Numerical data describing the outlet distributions and discrepancies between the approaches are listed in ESM Table S2.

The same exercise was carried out for programmed condition II. Figure 7 shows the predicted F_d (full curves, left axis) and S_d (dashed curves, right axis) for

Fig. 9 Predicted outlet number polydispersities $\sigma_d/\overline{d}_n$ as functions of t_r for programmed conditions I and II. *Full black curves* calculated from data in rows of t_r–d matrices. *Dashed red curves* correspond to $1/4F_d$. The *upper pair of curves* correspond to condition I and the *lower pair* to condition II. Predicted particle elution curves for conditions I and II are shown as *dash-dotted green* and *dashed blue curves*, respectively
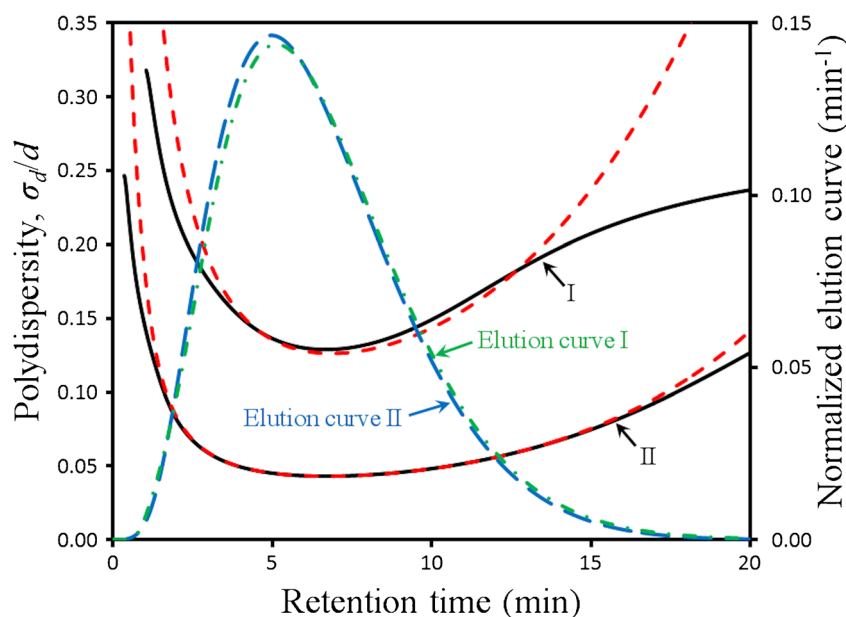
conditions I and II (red and black curves, respectively) as functions of $\log(d)$. The F_d for condition II is predicted to rise to a maximum of 5.81 at $d = 0.0094$ μm as compared to a maximum of 1.98 at the same particle size for condition I, as mentioned earlier. The S_d curves for the two conditions are very close for d between approximately 0.002 and 0.2 μm, as expected. In the case of condition I, S_d decreases below 0.002 μm, whereas for condition II S_d continues to increase until d falls to about 0.0008 μm, a result of the stronger retention of these smaller particles at the higher $\dot{V}_{c0}$ of condition II. Figure 8 shows the predicted outlet distribution curves at 2, 4, 6, 8, 10, and 12 min for condition II. As in Fig. 6, the distributions obtained using the time–diameter matrix approach are shown as full black curves and the predicted apparent Gaussian number distributions as dashed red curves. The outlet distributions in Fig. 8 are much narrower than those in Fig. 6 due to the higher F_d. Also, the agreement between the sets of curves in Fig. 8 is much better than in Fig. 6. The numerical data describing the outlet distributions of Fig. 8 are listed in ESM Table S3. Again, the greatest discrepancy between the approaches occurs at $t_r = 2$ min, but at the higher F_d of condition II, the monodisperse d eluting at mean t_r of 2 min differs only 1.5 % from $\overline{d}_n$, and $\sigma_{d,app}$ differs only 0.5 % from σ_d.

Finally, Fig. 9 shows plots of outlet polydispersities $\sigma_d/\overline{d}_n$ as functions of elution time, calculated using the data in rows of the respective t_r–d matrices for conditions I and II (full black curves). Plots of $1/4F_d$ for the two programmed conditions are shown as dashed red curves. Also included are the predicted normalized particle elution curves for conditions I and II shown as the dash-dotted green and dashed blue curves, respectively. These were obtained by summing the numbers of particles eluted across rows of the t_r–d matrices corresponding to the discrete elution times. These elution curves do not represent predicted fractograms of detector response versus time. To predict such a fractogram, contributions for each discrete particle size would have to be adjusted by the detector response function before summation at each discrete elution time. The particle elution curve for condition I is only very slightly broader than that for condition II. This is because the breadth is dominated by the assumed polydispersity of the sample. The values for $1/4F_d$ may be seen to serve very well as estimated upper bounds to outlet polydispersity for the two programmed conditions. For condition I, the $1/4F_d$ approximation slightly underestimates outlet polydispersity on the tail of the distribution, but for condition II the agreement is excellent across the full size distribution. Some discrepancy in the $1/4F_d$ approximation may be expected at the extremities of the distribution where the predicted F_d are lower. The effects described earlier associated with the skew of outlet distributions predicted by the t_r–d matrix are exacerbated at low F_d on the front and tail of the sample distribution.

Conclusions

The theory has been presented for predicting t_r and F_ϕ as functions of selective parameter ϕ for As-FlFFF where the cross flow rate as well as the inlet and outlet flow rates are allowed to vary with time. An estimation for the contribution to multipath bandspreading under programmed conditions was included where it was assumed that the multipath effect did not vary strongly along the channel length. It was shown that, under exponentially programmed decay of cross flow rate and constant outlet flow rate, the residual outlet polydispersity is very well approximated by $1/4F_\phi$. This confirms the importance of basing the optimization of programmed flow rate conditions on the predicted fractionating power. This is especially true when online MALS or DLS detection is used to extract particle size or molecular weight information from the eluent. The use of online MALS or DLS detection in combination with guidance in the selection of programmed conditions firmly based on fundamental FFF theory is recommended. The quantitative information provided by light scattering can correct for small perturbations from ideal FFF theory and uncertainties in instrumental parameters (channel thickness, channel volume, carrier fluid temperature and viscosity, etc.), while the maximization of fractionating power ensures that the light scattering information is obtained under optimum conditions. A variety of cross flow decay programs have been employed for sample analyses. It will now be possible to examine the utility of these different programs by a comparison of the predicted F_ϕ as functions of ϕ.

References

1. Yang FJF, Myers MN, Giddings JC. Programmed sedimentation field-flow fractionation. Anal Chem. 1974;46(13):1924–30. doi:10.1021/ac60349a009.
2. Kirkland JJ, Rementer SW, Yau WW. Time-delayed exponential field-programmed sedimentation field flow fractionation for particle-size-distribution analyses. Anal Chem. 1981;53(12): 1730–6. doi:10.1021/ac00235a005.
3. Giddings JC, Yang FJF, Myers MN. Flow field-flow fractionation: a versatile new separation method. Science. 1976;193(4259):1244–5. doi:10.1126/science.959835.

4. Giddings JC, Yang FJ, Myers MN. Theoretical and experimental characterization of flow field-flow fractionation. Anal Chem. 1976;48(8):1126–32. doi:10.1021/ac50002a016.

5. Lee HL, Lightfoot EN. Preliminary report on ultrafiltration-induced polarization chromatography—an analog of field-flow fractionation. Sep Sci. 1976;11(5):417–40. doi:10.1080/01496397608085333.

6. Granger J, Dodds J, Leclerc D, Midoux N. Flow and diffusion of particles in a channel with one porous wall: polarization chromatography. Chem Eng Sci. 1986;41(12):3119–28. doi:10.1016/0009-2509(86)85049-7.

7. Wahlund K-G, Giddings JC. Properties of an asymmetrical flow field-flow fractionation channel having one permeable wall. Anal Chem. 1987;59(9):1332–9. doi:10.1021/ac00136a016.

8. Wahlund K-G, Winegarner HS, Caldwell KD, Giddings JC. Improved flow field-flow fractionation system applied to water soluble polymers: programming, outlet stream splitting, and flow optimization. Anal Chem. 1986;58(3):573–8. doi:10.1021/ac00294a018.

9. Botana AM, Ratanathanawongs SK, Giddings JC. Field-programmed flow field-flow fractionation. J Microcolumn Sep. 1995;7(4):395–402. doi:10.1002/mcs.1220070412.

10. Ratanathanawongs SK, Giddings JC. Dual-field and flow-programmed lift hyperlayer field-flow fractionation. Anal Chem. 1992;64(1):6–15. doi:10.1021/ac00025a003.

11. Giddings JC, Williams PS, Beckett R. Fractionating power in programmed field-flow fractionation: exponential sedimentation field decay. Anal Chem. 1987;59(1):28–37. doi:10.1021/ac00128a007.

12. Williams PS, Giddings JC, Beckett R. Fractionating power in sedimentation field-flow fractionation with linear and parabolic field decay programming. J Liq Chromatogr. 1987;10(8–9):1961–98. doi:10.1080/01483918708066808.

13. Williams PS, Giddings JC. Power programmed field-flow fractionation: a new program form for improved uniformity of fractionating power. Anal Chem. 1987;59(17):2038–44. doi:10.1021/ac00144a007.

14. Williams PS, Giddings JC. Theory of field-programmed field-flow fractionation with corrections for steric effects. Anal Chem. 1994;66(23):4215–28. doi:10.1021/ac00095a017.

15. Martin M, Hoyos M. On the no-field method for void time determination in flow field-flow fractionation. J Chromatogr A. 2011;1218(27):4117–25. doi:10.1016/j.chroma.2011.01.010.

16. Litzén A, Wahlund K-G. Zone broadening and dilution in rectangular and trapezoidal asymmetrical flow field-flow fractionation channels. Anal Chem. 1991;63(10):1001–7. doi:10.1021/ac00010a013.

17. Williams PS. Design of an asymmetrical flow field-flow fractionation channel for uniform channel flow velocity. J Microcolumn Sep. 1997;9(6):459–67. doi:10.1002/(SICI)1520-667X(1997)9:6<459::AID-MCS3>3.0.CO;2-0.

18. Litzén A, Wahlund K-G. Improved separation speed and efficiency for proteins, nucleic acids and viruses in asymmetrical flow field flow fractionation. J Chromatogr. 1989;476:413–21. doi:10.1016/S0021-9673(01)93885-3.

19. Kirkland JJ, Dilks Jr CH, Rementer SW, Yau WW. Asymmetric-channel flow field-flow fractionation with exponential force-field programming. J Chromatogr. 1992;593(1–2):339–55. doi:10.1016/0021-9673(92)80303-C.

20. Moon M, Hwang I. Hydrodynamic vs. focusing relaxation in asymmetrical flow field-flow fractionation. J Liq Chromatogr Relat Technol. 2001;24(20):3069–83. doi:10.1081/JLC-100107720.

21. Moon MH. Frit-inlet asymmetrical flow field-flow fractionation (FI-AFlFFF): a stopless separation technique for macromolecules and nanoparticles. Bull Kor Chem Soc. 2001;22(4):337–48.

22. Moon MH, Williams PS, Kang D, Hwang I. Field and flow programming in frit-inlet asymmetrical flow field-flow fractionation. J Chromatogr A. 2002;955(2):263–72. doi:10.1016/S0021-9673(02)00226-1.

23. Andersson M, Wittgren B, Schagerlöf H, Momcilovic D, Wahlund K-G. Size and structure characterization of ethylhydroxyethyl cellulose by the combination of field-flow fractionation with other techniques. Investigation of ultralarge components. Biomacromolecules. 2004;5(1):97–105. doi:10.1021/bm030051z.

24. Leeman M, Wahlund K-G, Wittgren B. Programmed cross flow asymmetrical flow field-flow fractionation for the size separation of pullulans and hydroxypropyl cellulose. J Chromatogr A. 2006;1134(1–2):236–45. doi:10.1016/j.chroma.2006.08.065.

25. Williams PS. Fractionating power and outlet stream polydispersity in asymmetrical flow field-flow fractionation. Part I: isocratic operation. Anal Bioanal Chem. 2016;408(12):3247–63. doi:10.1007/s00216-016-9388-0.

26. Giddings JC. Displacement and dispersion of particles of finite size in flow channels with lateral forces. Field-flow fractionation and hydrodynamic chromatography. Sep Sci Technol. 1978;13(3):241–54. doi:10.1080/01496397808060222.

27. Williams PS. Retention ratio and nonequilibrium bandspreading in asymmetrical flow field-flow fractionation. Anal Bioanal Chem. 2015;407(15):4327–38. doi:10.1007/s00216-015-8734-y.

28. Giddings JC. Nonequilibrium theory of field-flow fractionation. J Chem Phys. 1968;49(1):81–5. doi:10.1063/1.1669863.

29. Giddings JC, Yoon YH, Caldwell KD, Myers MN, Hovingh ME. Nonequilibrium plate height for field-flow fractionation in ideal parallel plate columns. Sep Sci. 1975;10(4):447–60. doi:10.1080/00372367508058032.

30. Giddings JC. ERRATA. Displacement and dispersion of particles of finite size in flow channels with lateral forces. Field-flow fractionation and hydrodynamic chromatography. Sep Sci Technol. 1979;14(9):869–70. doi:10.1080/01496397908060246.

31. Giddings JC. Simplified nonequilibrium theory of secondary relaxation effects in programmed field-flow fractionation. Anal Chem. 1986;58(4):735–40. doi:10.1021/ac00295a018.

32. Hansen ME, Giddings JC, Schure MR, Beckett R. Corrections for secondary relaxation in exponentially programmed field-flow fractionation. Anal Chem. 1988;60(14):1434–42. doi:10.1021/ac00165a018.

33. Hakansson A, Magnusson E, Bergenståhl B, Nilsson L. Hydrodynamic radius determination with asymmetrical flow field-flow fractionation using decaying cross-flows. Part I. A theoretical approach. J Chromatogr A. 2012;1253:120–6. doi:10.1016/j.chroma.2012.07.029.

34. Magnusson E, Hakansson A, Janiak J, Bergenståhl B, Nilsson L. Hydrodynamic radius determination with asymmetrical flow field-flow fractionation using decaying cross-flows. Part II. Experimental evaluation. J Chromatogr A. 2012;1253:127–33. doi:10.1016/j.chroma.2012.07.005.

35. Press WH, Teukolsky SA, Vetterling WT, Flannery BP. Cubic spline interpolation. Numerical recipes in FORTRAN. The art of scientific computing. 2nd ed. Cambridge: Cambridge University Press; 1992. p. 107–10.

36. Nilsson L, Leeman M, Wahlund K-G, Bergenståhl B. Mechanical degradation and changes in conformation of hydrophobically modified starch. Biomacromolecules. 2006;7(9):2671–9. doi:10.1021/bm060367h.

37. Press WH, Teukolsky SA, Vetterling WT, Flannery BP. Integration of ordinary differential equations. Numerical recipes in FORTRAN. The art of scientific computing. 2nd ed. Cambridge: Cambridge University Press; 1992. p. 704.

38. Williams PS, Giddings MC, Giddings JC. A data analysis algorithm for programmed field-flow fractionation. Anal Chem. 2001;73(17):4202–11. doi:10.1021/ac010305b.

39. Giddings JC. 'Eddy' diffusion in chromatography. Nature. 1959;184(4683):357–8. doi:10.1038/184357a0.

40. Schure MR. Advances in the theory of particle size distributions by field-flow fractionation. Outlet and apparent polydispersity at constant field. J Chromatogr A. 1999;831(1):89–104. doi:10.1016/S0021-9673(98)00560-3.